CHAPTER 9

Reaction Thruster Attitude Control

9.1 Introduction

In Chapters 5–8, various control laws were presented for attitude stabilization and maneuvering. The hardware used to implement the control laws were principally momentum exchange devices as well as magnetic and solar torque controllers. Such controllers work in a linear continuous mode. The torques that they can provide are in the range of 0.02–1 N-m for momentum exchange devices, 10^{-2}–10^{-3} N-m for magnetic torque controllers, and 10^{-5}–10^{-6} N-m for solar torque controllers.

This form of attitude control has two major disadvantages. First, the speed of attitude maneuvering is limited by the low-level maximal torques that can be delivered to the ACS. The second but no less important difficulty was encountered in orbit-maneuvering tasks. The high-level liquid thrusters (or solid propulsion motors) used for orbit changes induce parasitic torques due to physical irregularities of the propulsion system. The level of induced parasitic torques is of the order of several newton-meters. The only way to control the attitude of the spacecraft under such disturbance conditions is to use reaction thruster controllers (see also Section 8.8).

Reaction thrusters used in attitude control are activated in a *pulsing mode* only. There are no linear, continuous reaction thrust controllers. This fact somehow complicates the analytical treatment of attitude control systems using them as torque controllers. However, they can provide almost any torque level, as surveyed in Appendix C. Reaction torque levels ranging between 0.01 N-m and 30 N-m are very common in most spacecraft. For practical considerations, it is convenient to use thrusters of the same thrust level for all control tasks in the satellite, but if this is not feasible then thrusters with different thrust levels can be incorporated as part of a unified propulsion system.

This chapter deals with the analysis and design of reaction thruster attitude control. It also covers two principal difficulties caused by the pulsing mode of thruster firing: the limits on attitude accuracy that can be achieved with a given thruster, and the fuel penalty associated with sensor noise. The quality of an ACS using propulsion torque controllers is strongly influenced by the specifications of the reaction thrusters; an introduction to propulsion hardware can be found in Appendix C.

9.2 Set-Up of Reaction Thruster Control

Reaction thrusters must be viewed in the context of a unified control system. In general, six thrusters are needed to allow attitude maneuvers in space, although some highly sophisticated systems claim to achieve the same space maneuvers with only four thrusters, strategically located on the satellite body (see Section 9.5). But for various practical reasons, six or more thrusters are necessary to complete a reaction control system.

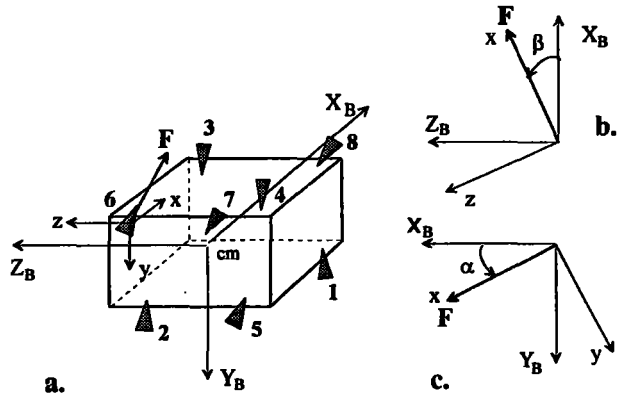

Figure 9.2.1 Eight-thruster arrangement, with direction details for thruster 6.

The level of torque that a reaction thruster can apply about a satellite axis depends not only on its thrust level but also on the torque-arm length about the axis. This statement suggests that correct thruster use depends primarily on its location on the satellite, and also on its inclination to the satellite body axes. Needless to say, different torque levels might be needed about the three principal body axes, so the location of the thrusters and their direction must be carefully studied before a final physical set-up is adopted for the propulsion system. The location and direction of the thrusters is also influenced by the location of the optical sensors and solar panels, which must not be damaged by the thrust flow. In the following analysis we will outline the different tradeoffs made in choosing the location of a thruster and the direction of its thrust axis relative to the body frame.

Figure 9.2.1 shows a potential arrangement of low-thrust satellite thrusters. First, it is clear that they must provide both positive and negative control torques about each of the satellite's body axes. (This arrangement is different from that in Figure 6.5.1, where e.g. thrusters TH2 and TH5 apply pure positive and negative torques about the $\mathbf{X}_B$ body axis.) In the next section we calculate the torque components applied by a thruster about each body axis as a function of the thruster's location and direction, denoted in the figure by the elevation and azimuth angles α and β, respectively.

9.2.1 *Calculating the Torque Components of a Single Thruster*

If the thrust vector is **F**, then the torque about the center of mass (cm) of the spacecraft will be $\mathbf{M} = \mathbf{r} \times \mathbf{F}$, where **r** is the vector distance of the thruster from the cm. The components of **r** are r_x, r_y, and r_z in the body axis frame; the thrust level is F. The direction of the thrust is defined by the elevation and azimuth angles α and β.

Suppose that initially **F** is in the direction of $\mathbf{X}_B$. After two rotations - first about the **y** axis of the thruster by an angle β, and then about the **z** axis of the thruster by an angle α - we find that the components of **F** along the body axes are

$$F_x = F\cos(\alpha)\cos(\beta), \quad F_y = F\sin(\alpha), \quad F_z = F\cos(\alpha)\sin(\beta). \tag{9.2.1}$$

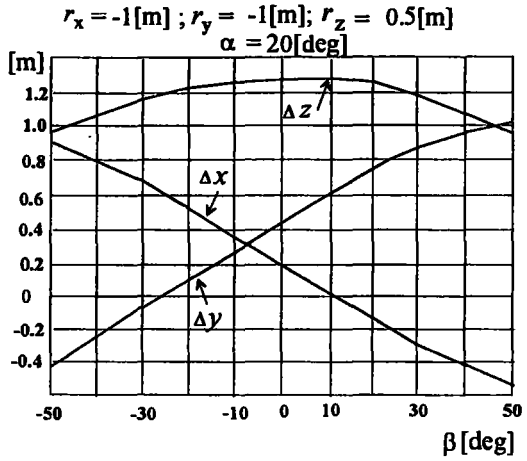

Figure 9.2.2 Equivalent torque arms for thruster 6.

The position r of the thruster can be expressed as:

$$\mathbf{r} = \mathbf{i}r_x + \mathbf{j}r_y + \mathbf{k}r_z. \tag{9.2.2}$$

With these relations, the torque components of **M** are

$$\mathbf{M} = \begin{bmatrix} M_x \\ M_y \\ M_z \end{bmatrix} = \mathbf{r} \times \mathbf{F} = \begin{bmatrix} r_y \sin(\beta)\cos(\alpha) - r_z \sin(\alpha) \\ r_z \cos(\alpha)\cos(\beta) - r_x \cos(\alpha)\sin(\beta) \\ r_x \sin(\alpha) - r_y \cos(\alpha)\cos(\beta) \end{bmatrix} F = \begin{bmatrix} \Delta x \\ \Delta y \\ \Delta z \end{bmatrix} F. \tag{9.2.3}$$

Equation 9.2.3 establishes the equivalent torque arms $\Delta x, \Delta y, \Delta z$ of the thrust **F** about the three body axes. Figure 9.2.2 exhibits the dependence of $\Delta x, \Delta y, \Delta z$ on the elevation and azimuth angles α and β for the location of thruster 6 at $r_x = -1$ m, $r_y = -1$ m, and $r_z = 0.5$ m; the value of the elevation angle is $\alpha = 20°$. Since $\alpha > 0$ (see Figure 9.2.1), Δz is always positive. But Δx and Δy can change sign, depending on the value of the azimuth angle β.

The importance of the results displayed in Figure 9.2.2 lies in the fact that the torque arms about any body axis can be decreased at will, thus enabling low torque levels even at relatively high-thrust levels. This in turn enables fine attitude control, but at the expense of low fuel efficiency.

Chapter 8 dealt with a number of control configurations in which the minimum impulse bit of a single reaction shot plays an important factor in achievable roll and yaw accuracies (see Eq. 8.8.6). The minimum impulse bit of the thruster is generally determined by the reaction thruster characteristics, and cannot be decreased at will. On the other hand, correct location and inclination of the thruster relative to the spacecraft body can decrease the minimum Δz as desired by affecting the equivalent torque arms of the thruster.

Most attitude control laws calculate the torques to be applied about the body axes. In Section 7.3.4 we learned how to distribute these torque commands to the four reaction wheels. The algorithm used to realize the torque transformation was very simple, as Eq. 7.3.26 showed.

The algorithm that transforms the command control torques about the body axes to reaction thruster activations is much more complicated, for two reasons. (1) Reaction thrusters are not linear controllers, since the level of the thrust output is constant. Consequently, the equivalent torque that the thruster will produce depends on the time period in which the thruster is activated. (2) A thruster is capable of producing one-signed torques only. In order to achieve a torque about the same axis with the opposite sign, a different thruster must be activated about the same axis in the opposite direction (see also Section 9.5). These two factors drastically complicate the algorithm that transforms body torque commands into thruster activation commands.

9.2.2 *Transforming Torque Commands into Thruster Activation Time*

This section describes a basic algorithm that uses the pulse width modulation principle to transform the torque commands into correctly timed activation of the relevant thrusters. The algorithm as described here is not optimized in terms of simplifying to a minimum its onboard version. We prefer to make the algorithm more comprehensible by showing clearly all its sequential operations.

The algorithm naturally depends on the physical set-up of the thrusters. We will base the demonstration algorithm on the set-up shown in Figure 9.2.3, which is a potential set-up for a geostationary satellite. The thrusters are arranged so that they provide the necessary torques for attitude control about the three body axes as well as the necessary thrust for station keeping. Thrusters 3–6 are used for N–S (inclination) SK (Section 3.5.1); thrusters 1 and 2 are used for E–W (longitude) SK (Section 3.4.4) and also for eccentricity corrections (Section 3.5.2).

In addition to station-keeping tasks, the set-up in Figure 9.2.3 allows for 3-DOF attitude control. Thrusters 1 and 2 provide the negative and the positive pitch control torques (respectively) about the $\mathbf{Y}_B$ axis; thruster 3 provides positive torque about the $\mathbf{X}_B$ axis but simultaneously a negative torque about the $\mathbf{Z}_B$ axis; and so on. Formally,

$$\begin{aligned} Ty+ &= Th2, & Ty- &= Th1; \\ Tx+ &= Th3+Th5, & Tx- &= Th4+Th6; \\ Tz+ &= Th5+Th6, & Tz- &= Th3+Th4. \end{aligned} \tag{9.2.4}$$

Here the + and − signs indicate the sign of the produced torques about the body axes, and *Thi* denotes thruster *i*.

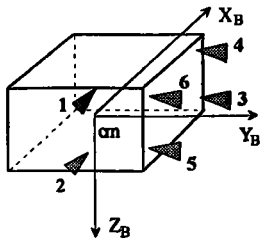

Figure 9.2.3 Possible thruster set-up for a geostationary satellite.

In order to simplify our analysis, the thrusters are located symmetrically about the body axes, with equal torque arms about the same axis; the directions of the thruster axes are parallel to the body axes. The torque efficiency of each thruster depends on the thrust level F, and also on the torque arms $\Delta x, \Delta y, \Delta z$ (Section 9.2.1). We define the torque constants as $G_X = F\Delta x$, $G_Y = F\Delta y$, and $G_Z = F\Delta z$. With this notation, we can express the torques about the body axes as

$$\begin{aligned} Tx &= [Th5 + Th3 - Th4 - Th6]G_X, \\ Tz &= [Th5 + Th6 - Th3 - Th4]G_Z, \\ Ty &= [Th2 - Th1]G_Y. \end{aligned} \tag{9.2.5}$$

Since the produced torques are momentarily determinated by G_X, G_Y, and G_Z, the *average torque* provided during a sampling time depends upon the time that the thrusters are *on* relative to the sampling time T_{sam}. This is the principle of pulse width modulation (PWM), which is treated in subsequent sections. First, we normalize the body control torques to

$$\hat{T}x = \frac{Tx}{G_X}, \quad \hat{T}y = \frac{Ty}{G_Y}, \quad \hat{T}z = \frac{Tz}{G_Z},$$

and define Ti as the ratio between the thruster "on-time" and the sampling time for thruster Thi. Thus the first two of Eqs. 9.2.5 can be rewritten in the following form:

$$\begin{bmatrix} \hat{T}x \\ \hat{T}z \end{bmatrix} = \begin{bmatrix} 1 & -1 & 1 & -1 \\ -1 & -1 & 1 & 1 \end{bmatrix} \begin{bmatrix} T3 \\ T4 \\ T5 \\ T6 \end{bmatrix}. \tag{9.2.6}$$

(This is similar to Section 7.3.4, where four reaction wheels were used to provide torques about three body axes.) Although the matrix of Eq. 9.2.6 is not square, it does have a right pseudoinverse, yielding

$$\begin{bmatrix} T3 \\ T4 \\ T5 \\ T6 \end{bmatrix} = \frac{1}{4} \begin{bmatrix} 1 & -1 \\ -1 & -1 \\ 1 & 1 \\ -1 & 1 \end{bmatrix} \begin{bmatrix} \hat{T}x \\ \hat{T}z \end{bmatrix}. \tag{9.2.7}$$

According to the values of $\hat{T}x$ and $\hat{T}z$, Ti can have negative values, which cannot be physically realized with the thruster i. A negative on-time means that a torque of opposite sign is to be produced with thruster Thi, which is not physically possible. This situation can be remedied by activating, for an identical duration, another thruster providing the same torque but with a *positive* on-time. For instance, in Figure 9.2.3, suppose that $T3$ comes out to be negative. In this case, $Th6$ should be activated instead for the same on-time $T3$, assuming that the Δx and Δz torque arms of $Th3$ and $Th6$ are equal.

If the torque arms are not equal then G_X, G_Y, G_Z must be defined separately for each thruster, and Eqs. 9.2.5 must be rewritten accordingly. The algorithm is listed as follows.

$T3 = [+\hat{T}_x - \hat{T}_z]/4$
$T4 = [-\hat{T}_x - \hat{T}_z]/4$
$T5 = [+\hat{T}_x + \hat{T}_z]/4$
$T6 = [-\hat{T}_x + \hat{T}_z]/4$

$TT6 = T6 - T3$; $TT3 = 0$

IF($TT6$.LT.0) THEN $TT3 = T3 - T6$; $TT6 = 0$

$TT4 = T4 - T5$; $TT5 = 0$

IF($TT4$.LT.0) THEN $TT5 = T5 - T4$; $TT4 = 0$
IF($\hat{T}_y$.GT.0) THEN $TT2 = \hat{T}_y$; $TT1 = 0$
IF($\hat{T}_y$.LT.0) THEN $TT1 = \text{Abs}(\hat{T}_y)$; $TT2 = 0$

Here TTi stands for the time duration of the *on* condition for each thruster i. In essence, the algorithm realizes a kind of pulse width modulation, upon which many pulsed attitude control schemes are based.

Algorithms for other reaction thruster set-ups, such as those shown in Figure 9.2.1 and Figure 6.5.1, can be written in a similar way. With asymmetrical location of the thrusters and different thrust levels or directions of their thrust axes, the algorithm might become quite complicated. Still, the technique of formulating it remains the same. The following sections deal with realization of attitude control loops based on the reaction thruster set-up of Figure 9.2.3.

9.3 Reaction Torques and Attitude Control Loops

9.3.1 *Introduction*

The control laws to be used for reaction attitude control loops are the same laws treated in Section 7.2. Unfortunately, reaction controllers do not possess the same linear relationship between the input to the controller and its output torque. In fact, they are activated in an on-off mode. Nonetheless, they can be used in a quasi-linear mode by modulating the width of the activated reaction pulse proportionally to the level of the torque command input to the controller. This is the often used *pulse width modulation* (PWM) principle. A related design technique is based on the well-known Schmidt trigger, which implements a *pulse width-pulse frequency modulation* (PWPFM) in which the distance between the pulses is also modulated. Both modulation techniques will be analyzed in this chapter as part of attitude feedback control loops.

By definition, attitude control loops based on reaction controllers are *sampled,* with all the implications attendant upon such systems. There are numerous automatic control textbooks dealing with sampled control systems; see for instance Saucedo and Schiring (1968), Kuo (1970), Franklin and Powell (1980), Houpis and Lamont (1985), or D'Azzo and Houpis (1988).

With certain assumptions, the "area" of the reaction pulse can be approximated as an impulse (Figure 9.3.1, overleaf). This allows the feedback control loops to be analyzed as a conventional digital control system, for which the classical tools of automatic control theory hold. Design techniques based on the Nyquist, Bode, Nichols,

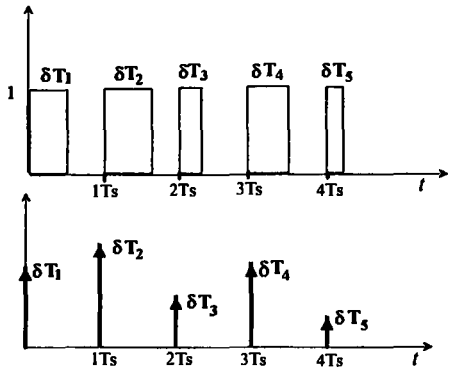

Figure 9.3.1 Approximation of PW-modulated pulses to impulses.

and root-locus theories apply nicely to these systems, as we shall see in the present chapter. There is, however, a significant deficiency in sampled systems. The bandwidth of the closed loop that can be achieved is limited – in a very determined way – by the sampling time (Sidi 1980).

9.3.2 *Control Systems Based on PWPF Modulators*

Apparently owing to technical heritage from the "analog age" of onboard computers, pulse width–pulse frequency modulators are still predominant in attitude and orbit control systems (AOCS). They emerged from the widely used analog monostable Schmidt trigger, a basic element in analog pulse techniques (Millman and Taub 1956, Joice and Clarke 1961).

The standard practical realization of a PWPF modulator control loop is shown in Figure 9.3.2, where K_x and K_{xd} are the usual proportional and derivative gains. The dynamics of the sensor and of the sensor noise filter have been omitted in order to simplify the analysis. The attitude and its derivative errors (*Er* in the figure) are transformed into a burst of idealized rectangular pulses.

Figure 9.3.2.b shows a variation of the PWPF modulator, the so-called pseudo rate (PR) modulator. Its special characteristic lies in the fact that the time-constant network is located in the feedback path of the modulator, thus giving the modulator "lead–lag" compensating abilities. Because of the dead-zone region of the hysteresis block, the lead phase is achieved with a lesser amplification of the sensor noises at the input to the modulator. For stabilization of spacecraft with large flexible appendages, control and modulator parameters must be carefully matched to ensure stability of structural modes of vibration (Bittner, Fisher, and Surauer 1982).

A detailed analysis of the PWPF modulator follows. Our aim is to obtain a relationship between the input $Er = In$ and the frequency- and width-modulated values of the output pulse sequence, characterized by the *on* and *off* time periods.

Calculating t_{on} and t_{off} for the PWPF Modulator

The calculation of these variables is based on the time behavior shown in Figure 9.3.3. Our presentation will be broken down into five steps.

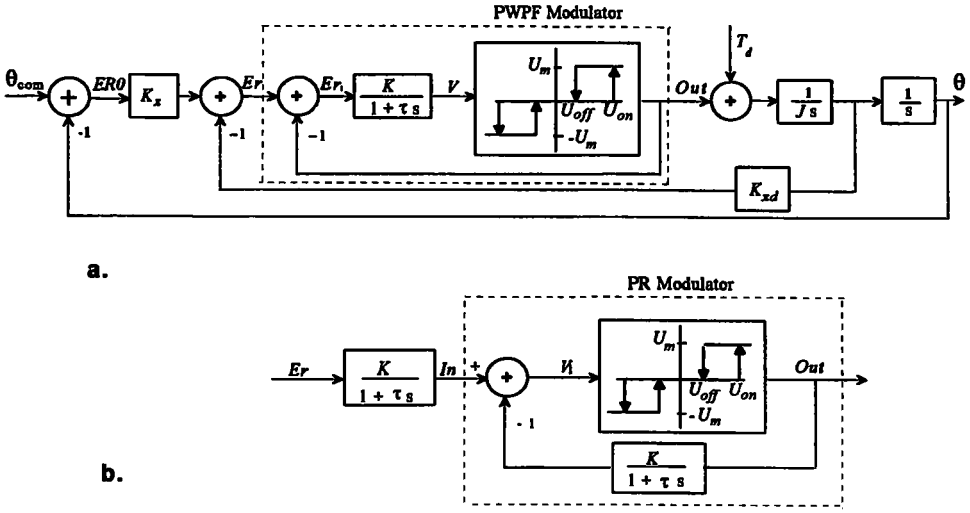

Figure 9.3.2 Basic attitude control loops using PWPF and PR modulators; adapted from Bittner, Fisher, and Surauer (1982) by permission of IFAC.

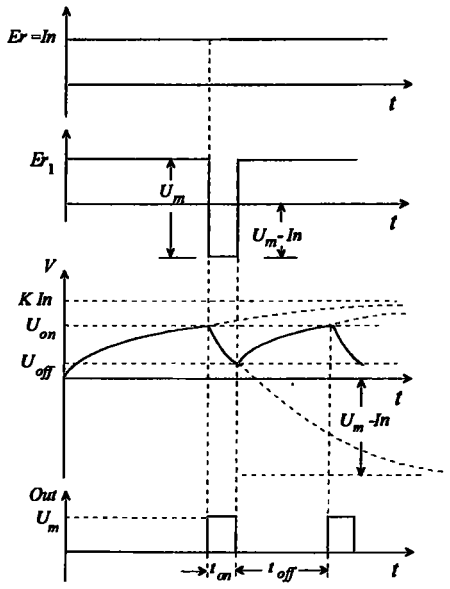

Figure 9.3.3 Time behavior of the PWPF modulator used for calculating t_{on} and t_{off}.

(1) As long as $V < U_{on}$, the system is quiet. The effective dead zone is U_{on}/K, where K is the DC gain of the time constant network of the modulator (Figure 9.3.2.a). The hysteresis block in the figure is the Schmidt trigger. The smallest input that can activate the hysteresis block is

$$In = U_{on}/K. \tag{9.3.1}$$

(2) Compute the time behavior of V as a result of Er_1. The dynamic equation is simply

$$\dot{V}\tau + V = KEr_1. \tag{9.3.2}$$

Taking the Laplace transform of this equation, we obtain

$$V(s) = \frac{\tau V(0)}{1+s\tau} + \frac{KEr_1}{s(1+s\tau)}. \tag{9.3.3}$$

The time-domain solution is simply

$$V(t) = V(0)e^{-t/\tau} + KEr_1[1-e^{-t/\tau}]. \tag{9.3.4}$$

(3) We now compute t_{on}. According to Figure 9.3.2, $V(t)$ starts at U_{on} and decreases asymptotically to $In - U_m$, which means that $V(0) = U_{on}$ and $KEr_1 = K(In - U_m)$. This decrease will stop at U_{off}, so that

$$\begin{aligned} U_{off} = V &= U_{on}e^{-t_{off}/\tau} + K(In - U_m)(1-e^{-t_{on}/\tau}) \\ &= K(In - U_m) + (U_{on} - KIn + KU_m)e^{-t_{on}/\tau}. \end{aligned} \tag{9.3.5}$$

It follows that

$$e^{-t_{on}/\tau} = \frac{U_{off} - KIn + KU_m}{U_{on} - KIn + KU_m} = 1 - \frac{U_{on} - U_{off}}{U_{on} - KIn + KU_m}. \tag{9.3.6}$$

For small t_{on}, $e^{-t_{on}/\tau} \approx 1 - t_{on}/\tau$. This yields the first-order approximation

$$t_{on} \approx \tau \frac{U_{on} - U_{off}}{KU_m - KIn + U_{on}}. \tag{9.3.7}$$

(4) To calculate t_{off} we first observe that, according to Figure 9.3.2, $V(t)$ tends toward KIn; it starts at $V(0) = U_{off}$ but its increase is halted at U_{on}. Hence we have

$$V(t) = e^{-t_{off}/\tau}U_{off} + KIn(1-e^{-t_{off}/\tau}) = U_{on}, \tag{9.3.8}$$

from which follows the final result:

$$e^{-t_{off}/\tau} = \frac{U_{on} - KIn}{U_{off} - KIn} = \frac{KIn - U_{on} + U_{off} - U_{off}}{KIn - U_{off}} = 1 - \frac{U_{on} - U_{off}}{KIn - U_{off}}. \tag{9.3.9}$$

For small t_{off}, a first-order approximation may likewise be used:

$$t_{off} \approx \tau \frac{U_{on} - U_{off}}{KIn - U_{off}}. \tag{9.3.10}$$

Some results concerning the time-domain behavior of the PWPF modulator with respect to our analytical equations are shown in Figure 9.3.4 and Figure 9.3.5. Figure 9.3.5.c (page 270) shows the resulting average output torque due to the input to the PWPF modulator in Figure 9.3.4.a. Except for the scaling factor of both input and output, the output adequately follows the input, as predicted. If we wish to use the reaction system with a lower fuel penalty, then wider pulses have some advantage because they have a higher average specific impulse I_{sp}. According to Eq. 9.3.7 and 9.3.10, the ratio t_{on}/t_{off} becomes larger if U_{off} is zeroed.

(5) Equation 9.3.6 and Eq. 9.3.9 (or the simplified Eq. 9.3.7 and Eq. 9.3.10) can be used to determine the five modulator parameters K, τ, U_{on}, U_{off}, and U_m. It is imper-

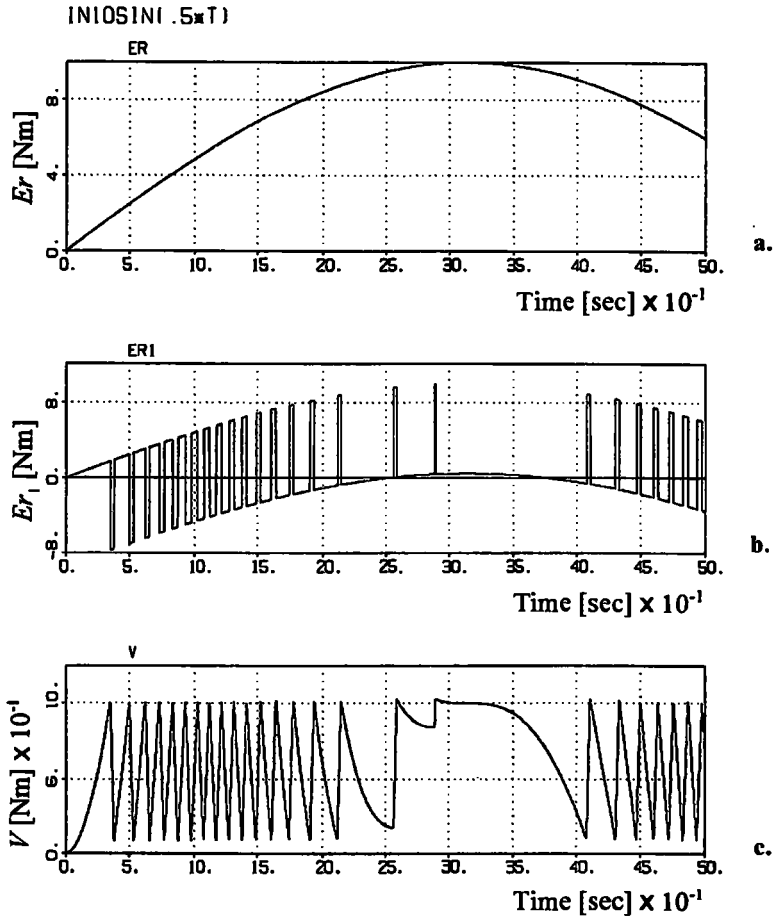

Figure 9.3.4 Time histories of the input and of the internal variables of the PWPF modulator.

ative to determine t_{on} and t_{off} based on physical considerations. The hysteresis coefficients are also important in determining the minimum dead zone that will give sufficient immunity to the sensor noise reaching the modulator input.

EXAMPLE 9.3.1 A PWPF modulator is implemented in a single-axis attitude control loop. The control gains K_x and K_{xd} in Figure 9.3.2 are chosen so that the control system has a closed-loop natural frequency of $\omega_n = 1$ rad/sec and a damping coefficient of $\xi = 1$. To satisfy some practical engineering requirements, the modulator parameters were chosen as follows: $K = 2$, $\tau = 0.5$, $U_{on} = 1$, $U_{off} = 0.1$, $U_m = 9.5$.

Figure 9.3.6 (page 271) shows the time responses for an angular input of 0.2°. The input *Er* and the output (*Out*) of the modulator are also shown on Figure 9.3.6. Figure 9.3.7 (page 272) shows the time response for an input of 1°.

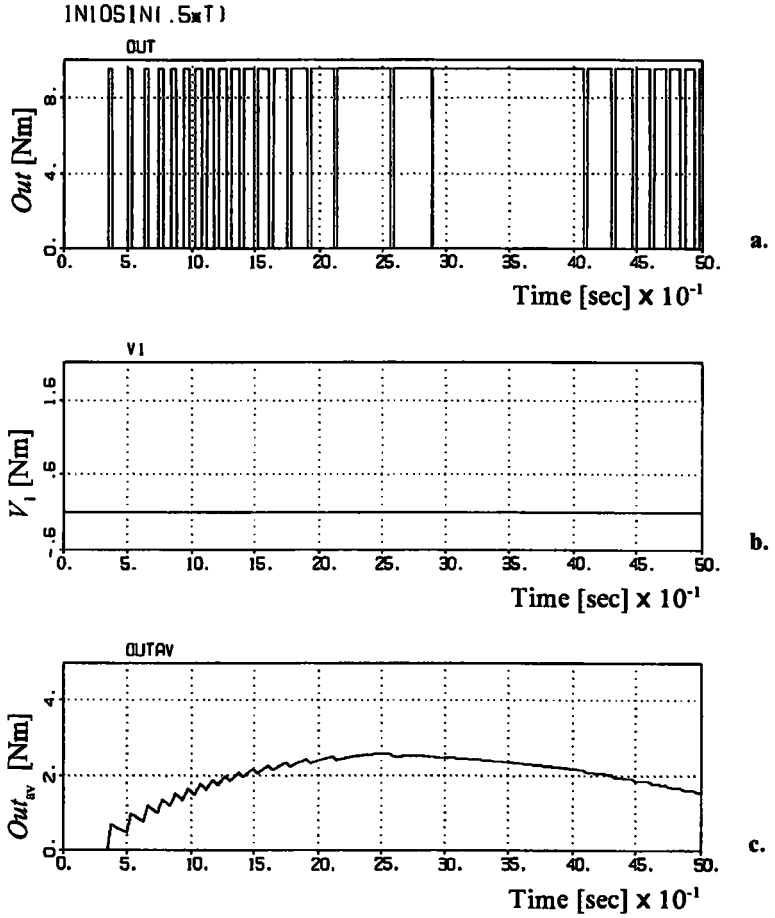

Figure 9.3.5 Output pulses and their average value of the PWPFM.

Calculating t_{on} and t_{off} for the PR Modulator

An analysis similar to that carried out for the PWPF modulator leads to the following results:

$$t_{on} = \tau \ln \frac{K U_m - In + U_{on}}{K U_m - In + U_{off}}, \tag{9.3.11}$$

$$t_{off} = \tau \ln \frac{In - U_{off}}{In - U_{on}}. \tag{9.3.12}$$

Equation 9.3.11 and Eq. 9.3.12 can be used to determine the parameters of the pseudo rate pulse modulator for efficient use in reaction attitude control systems.

9.3.3 *Control Loop Incorporating a PWPF Modulator*

Even though PWPF modulators are by definition nonlinear, they are easily incorporated in attitude control loops, whereupon the entire feedback control loop

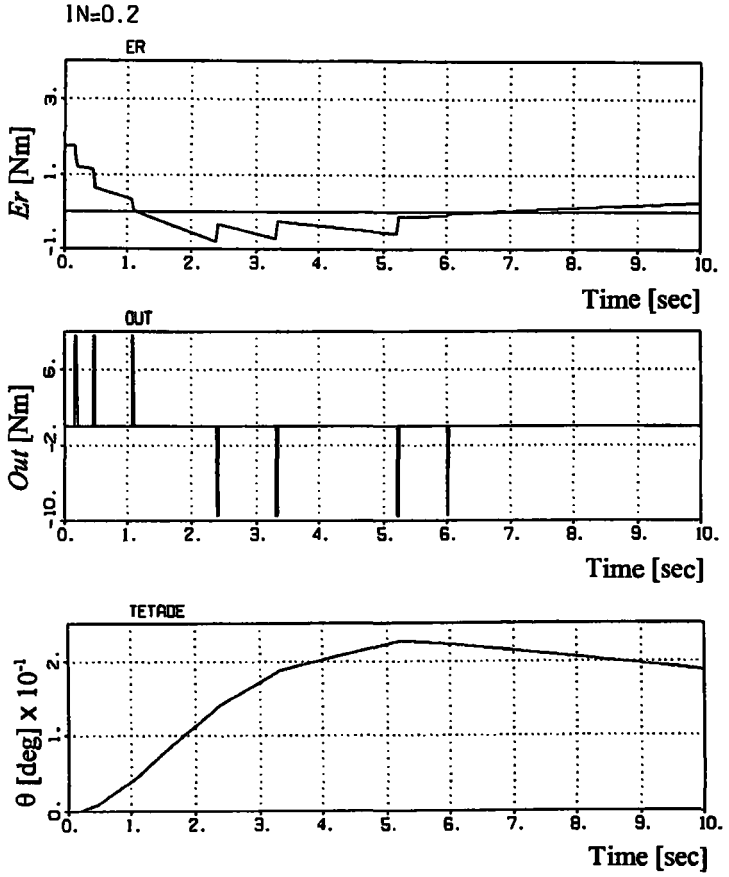

Figure 9.3.6 Time behavior of a PWPF modulator realization of an attitude control feedback loop, with an input of 0.2°.

can be analyzed by linear control theory. As can be seen from Figure 9.3.4.a and Figure 9.3.5.c, the average output of the modulator tracks the input quite accurately. In fact, the input-output characteristics of pulse modulators can be represented as in Figure 9.3.8 (see also Wie and Plescia 1984). Figure 9.3.8 (overleaf) shows the linear behavior of the modulator input-output characteristics except at very low and high inputs, where the nonlinear characteristics are purposely introduced to solve practical problems of sensor noise and to limit structural oscillation of panels and fuel slosh in a limit cycling mode (Vaeth 1965, Bittner et al. 1982).

Analog implementation of PWPF modulators is straightforward because analog (continuous) electronics technology is the natural medium for realizing these modulators, implemented by the Schmidt trigger scheme. However, PWPF modulation causes some practical problems with today's onboard microprocessors. Digital microprocessors work in a synchronous timing created by an electronic clock: the onboard computer sends control commands at equal time intervals, and pulse frequency modulation cannot be easily implemented. The equations of the previous section become invalid for a *discrete* "pulse frequency" modulator. This kind of modulator,

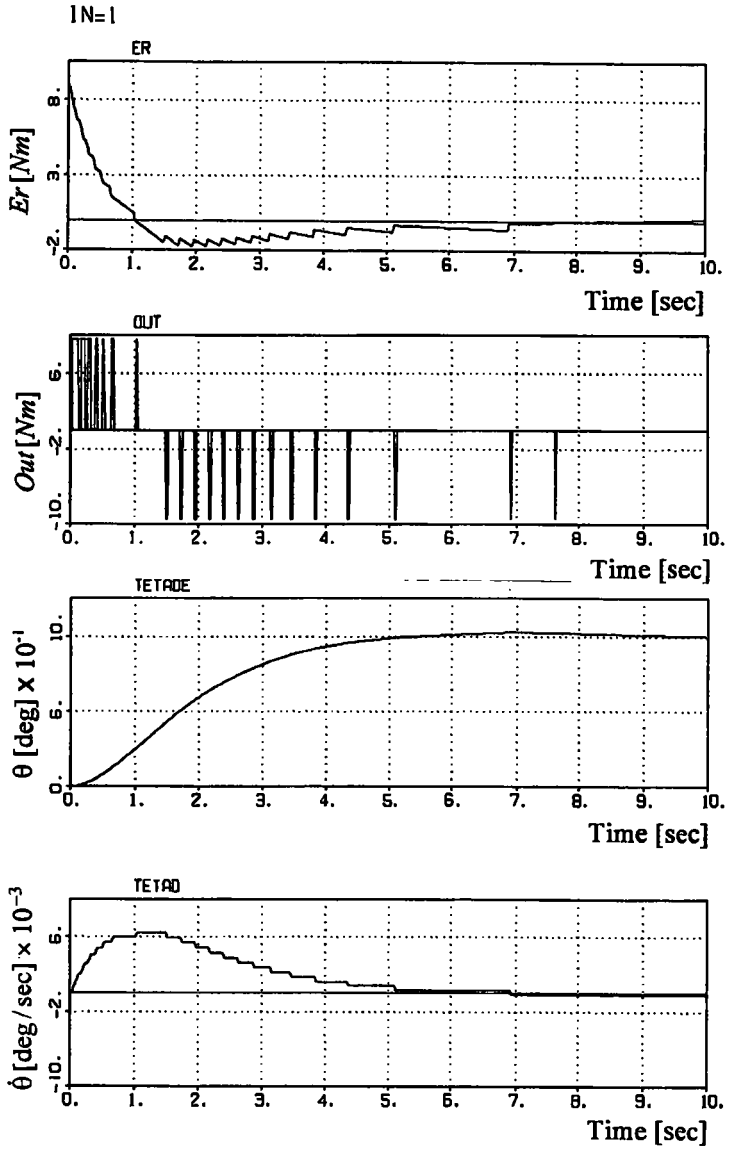

Figure 9.3.7 Time behavior of a PWPF modulator realization of an attitude control feedback loop, with an input of 1°.

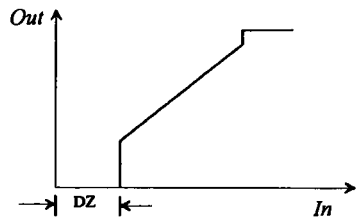

Figure 9.3.8 Input-output characteristics of a PWPF modulator.

when used in an onboard microprocessor, must be synchronized with the sampling time of that processor. Digital implementation of a PWPF modulator was the subject of a Ford Aerospace patent application (Chan 1982).

The nice characteristics that could be achieved with PWPF modulators are complicated by the practical difficulties just mentioned. It seems that, from the basic perspective of input-output characteristics, modulators based solely on pulse width modulation are simpler to apply in a microprocessor-based onboard computer. Attitude feedback control loops based on PWM will be analyzed in the next section.

9.4 Reaction Attitude Control via Pulse Width Modulation

9.4.1 *Introduction*

There are no fundamental differences between reaction pulse control loops using pulse width-pulse frequency modulation (PWPFM or PRM) and pulse width modulation (PWM). Both are based on the Schmidt trigger, but there do exist small differentiating nuances between these two kinds of control schemes.

In attitude feedback control loops based on PWM, the sampling frequency is constant and the reaction pulses are applied at equal time intervals. If the dynamics of the plant contains additional structural dynamics with low damping coefficients and eigenfrequencies equal to the sampling frequency of the control loop, then the structural dynamics might be excited, thus degrading the quality of the feedback control loop. Special precautions, such as adequate structural filters, must be incorporated to account for this phenomenon.

9.4.2 *Feedback Control Loop of a Pulsed Reaction System*

In previous chapters, in order to simplify the theoretical analysis, controllers were presumed to be analog. With today's technology, onboard control computers are no longer analog, and all feedback control loops are of the sampled type. For such continuous devices as reaction wheels or magnetic torque controllers, the onboard microprocessor approximates continuousness via a sampler followed by a *zero-order hold device.* With a sampling frequency that is reasonably high with respect to the bandwidth of the open-loop transfer function, the zero-order hold output is quasicontinuous. The sampler and the zero-order hold circuit have the net effect of adding some delay to the open-loop transfer function of the feedback system, which should be taken into consideration when designing with continuous control analysis techniques; design with discrete (digital) control techniques automatically takes care of this inherent delay. With *pulsed controllers,* in which a zero-hold device does not exist, the analysis and design must be carried out using discrete control techniques.

The basic control scheme of a pulsed attitude feedback control loop about one body axis is shown in Figure 9.4.1 (overleaf). With ideal torque impulses, the block of the PWM can be omitted. In this way, linear analysis of the sampled control loop is performed in the usual manner. With small *on* periods (as compared to the sampling period) of the reaction thrusters, omission of the PWM block is justified. This means that the amplitude of the impulses at the output of $G_1(z)$ and of $G(z)$ in Fig-

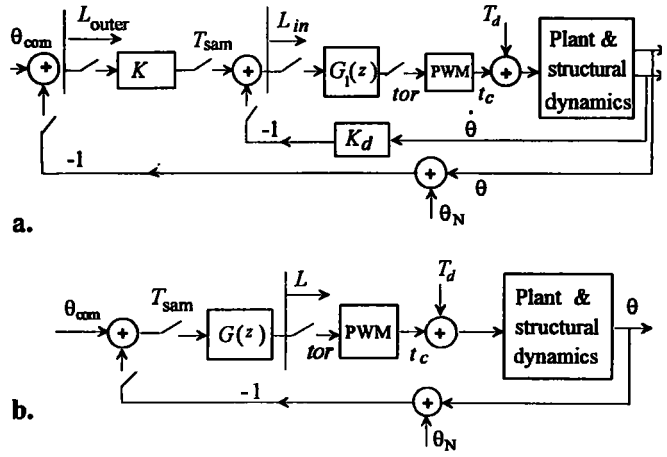

Figure 9.4.1 Pulsed controller attitude feedback control loop.

ure 9.4.1.a and Figure 9.4.1.b (respectively) takes the value of the rectangular pulses $F\Delta(\Delta t)$ of Section 9.2.2, where Δ is the torque arm and Δt is the pulse width.

Figure 9.4.1.a shows the most general block diagram for a single-axis attitude control loop in which the attitude and their derivatives can both be measured. Here K and K_d are the usual position and derivative controller gains, and $G_1(z)$ contains the required structural mode control networks, sensor noise filters, and an integrator (if one is needed to nullify the steady-state error to disturbances or to attitude command inputs). As mentioned previously, unless precise attitude control is imperative there is a tendency to avoid continuous use of rate sensors, such as the common rate gyro. In this case, the scheme of Figure 9.4.1.b is relevant, with the self-evident disadvantage of increasing the sensitivity of the system to position sensor noise.

The term T_d denotes the equivalent disturbance torque, comprising internal and external parasitic torques whose sources are irregularities in or bad modeling of the reaction thrusters, uncertainties in knowledge of the vehicle mass properties, and so forth. For instance, in the ABM stage - in which the transfer orbit is to be circularized at the apogee - a large disturbance torque may be present if the high-thrust vector does not pass exactly through the satellite's center of mass. The attitude reaction control loop must counteract this disturbance torque in order to prevent a large attitude error of the satellite, which would cause an incorrect ΔV increment (see Section 3.4.3). Another example of the importance in decreasing ACS sensitivity to T_d is in the N-S station keeping of geostationary satellites. Keeping the inclination of the orbit inside permitted limits is achieved by adding linear velocity increments to the s/c perpendicularly to its orbit (as explained in Section 3.5.1). During this stage, which may continue for several minutes, the satellite attitude error cannot exceed permitted tolerances without degrading the communication mission. In today's communications satellites, attitude error tolerances are of the order of 0.03°-0.1°, a difficult standard for the control engineer to achieve.

Naturally, an increase in the gain bandwidth of the control loop will decrease the attitude errors due to the external disturbances, but the existence of structural

dynamics will preclude very high loop gains. Hence, a careful design must procure the highest possible gains while still keeping the necessary gain and phase margins for the structural dynamics, including stability of the sloshing modes (see also Section 7.3.6). Another important control aspect is the behavior of the attitude output θ to control input θ_{com}. For all attitude control tasks, sensor noise is an important factor to be taken into account. For the set-up of Figure 9.4.1.b, in which it is assumed that no rate sensor is included in the control hardware, the noise of the position sensor might be strongly amplified; this precludes high open-loop gains (see also Section 7.3.6).

Sensitivity to External Disturbances

At the beginning of the analysis we shall assume that there are no structural filters, $G_1(z) = 1$ in Figure 9.4.1.a. We also know that, with no structural dynamics in the plant block, the simplified plant reduces to $P(s) = 1/Js^2$, where J is the satellite's moment of inertia. Also, without the pulse width modulator in the loop, PWM = 1. If we assume that the disturbance T_d is a continuous and constant step function with an amplitude of D, then

$$\theta(z) = \frac{DT_{sam}^2(z/2)(z+1)}{J(z-1)^3 + T_{sam}z(z-1)\left(K + K_d\frac{z-1}{z}\right)}, \tag{9.4.1}$$

where T_{sam} is the sampling time and z is the Z transform variable. Using the final-value theorem for sampled systems, the steady-state value of the output amounts to

$$\lim_{n\to\infty} \theta(nT_{sam}) = \lim_{z\to 1} \frac{z-1}{z}\theta(z) = \frac{DT_{sam}}{K} \tag{9.4.2}$$

and finally

$$TF_d = \frac{\theta_{ss}}{D} = \frac{T_{sam}}{K}. \tag{9.4.3}$$

Equation 9.4.3 shows that the steady-state error of the output angle θ depends on both the sampling time T_{sam} and the DC gain K. This gain is itself determined by the closed-loop natural frequency ($K = \omega_n^2 J$), and K_d is proportional to the damping coefficient ($K_d = 2\xi\omega_n J$). For the magnitude of the sensitivity ratio TF_d see Table 9.4.1, in which $J = 500$ kg-m^2 and $\xi = 0.7$.

Table 9.4.1 *Steady-state error as function of the sampling time and the closed-loop bandwidth*

ω_n [r/s]	K	K_d	T_{sam}[sec]	TF_d [rad/N-m]	D [N-m]	θ_{ss} [deg]
0.5	125	350	1.0	8.10^{-3}	1	0.46
0.5	125	350	0.5	4.10^{-3}	1	0.23
0.5	125	350	0.25	2.10^{-3}	1	0.114
0.25	31.25	175	1.0	32.10^{-1}	1	1.83
0.25	31.25	175	0.5	16.10^{-3}	1	0.92
0.25	31.25	175	0.25	8.10^{-3}	1	0.46

In this analysis of the discrete feedback control loop, the outputs of $G_1(z)$ or $G(z)$ in Figure 9.4.1 are impulses of amplitude *tor*, proportional to the processed attitude error. In practice, thrusters supply torques of constant amplitude and varying time length:

$$tp = tor/F\Delta, \tag{9.4.4}$$

where F is the thrust level and Δ the torque arm. This time transformation is performed with the PWM included in Figure 9.4.1.

In order to prevent exaggerated detrimental influence of sensor noise on control system performance, at least one first-order filter must be incorporated into the feedback control loop. The time constant of the filter must be low enough to leave the control loop with satisfactory gain and phase margins. Using the Tustin transformation to render the analog control network $G(s)$ discrete, we obtain

$$G(z) = \frac{KT_{sam} + 2k_d + (kT_{sam} - 2k_d)z^{-1}}{T_{sam} + 2\tau + (T_{sam} - 2\tau)z^{-1}}. \tag{9.4.5}$$

EXAMPLE 9.4.1 In this example, $\omega_n = 0.5$, $\xi = 0.7$, $J = 500$ kg-m^2, and either $T_{sam} = 0.25$ sec or $T_{sam} = 1$ sec; the disturbance $D = 1$ N-m. Using conventional frequency design techniques, the time constant of the filter was fixed to $\tau = 0.3$, with the resulting open-loop transfer function shown in Figure 9.4.2. The time-domain simulation results are shown in Figures 9.4.3 and 9.4.4 for a T_{sam} of 0.25 sec and of 1 sec, respectively. The steady-state error for the case with $T_{sam} = 0.25$ sec is 0.11°, as per Eq. 9.4.2. In Figure 9.4.4, with $T_{sam} = 1$ sec, the steady-state angular error is 0.456°; this also satisfies Eq. 9.4.2.

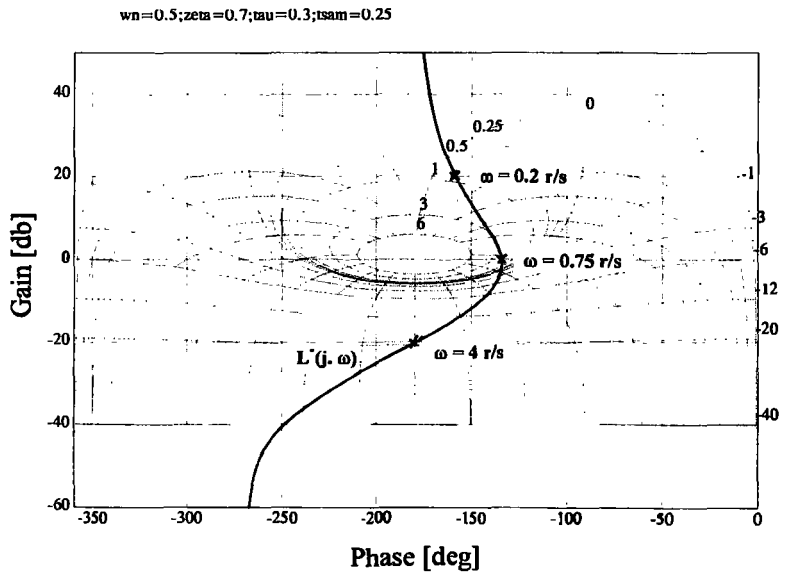

Figure 9.4.2 Open-loop transfer function on the Nichols chart for Example 9.4.1.

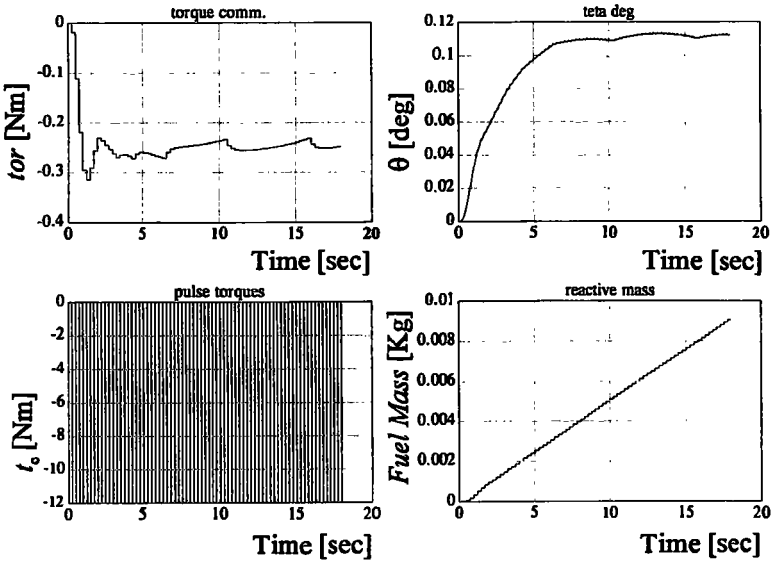

Figure 9.4.3 Time-domain results for the case with $T_{sam} = 0.25$ sec.

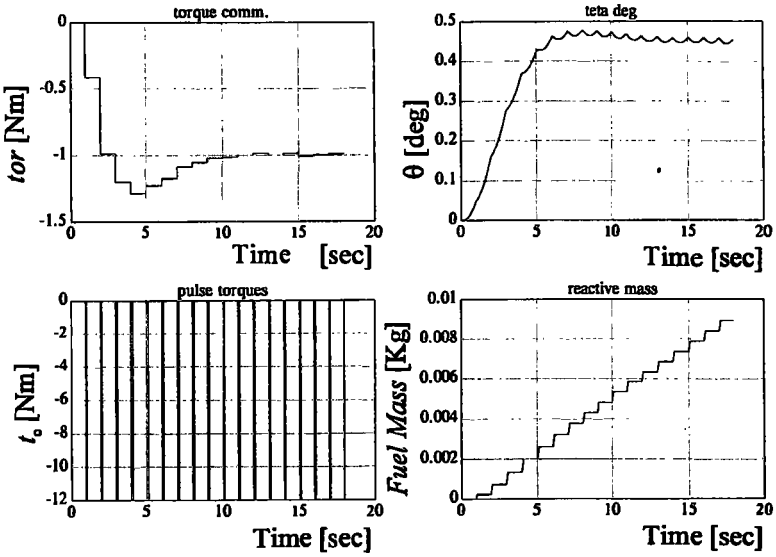

Figure 9.4.4 Time-domain results for the case with $T_{sam} = 1$ sec.

Equation 9.4.2 shows that the steady-state error depends on the sampling time T_{sam}. However, it would be more convenient to have a control law in which the steady-state error is *not* dependent on the sampling time. This is easily accomplished by arguing as follows. With a zero-order hold device, the processed output of the control network $G(z)$ is constant during the complete sampling period; thus, an angular momentum ($T_{sam}tor$) is delivered to the satellite. It is suggested that the reaction thruster deliver the same angular momentum, which means: $tp \times F\Delta = T_{sam}tor$, or

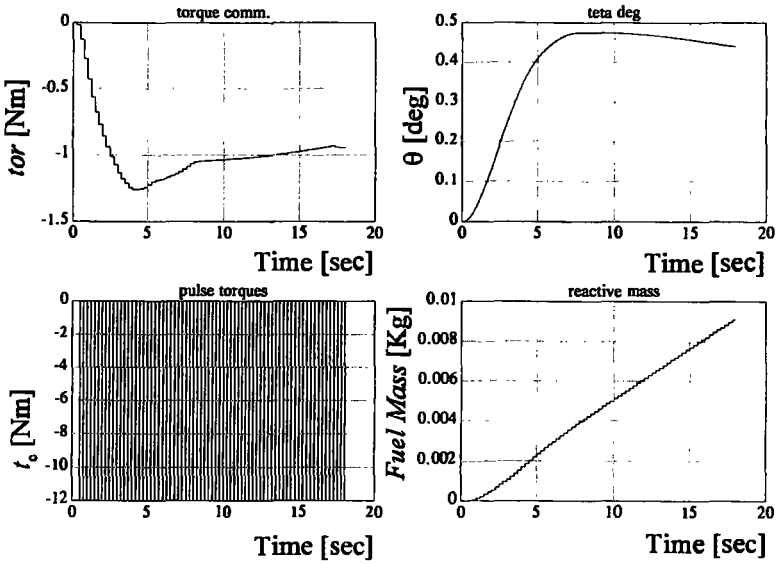

Figure 9.4.5 Time-domain results for the control system based on a PW modulator that renders the steady-state error independent of the sampling time T_{sam}.

$$tp = T_{sam} tor/F\Delta, \tag{9.4.6}$$

where *tor* is the commanded torque. The effect is equivalent to multiplying $G(z)$ by T_{sam}. With this assumption, Eq. 9.4.1 and Eq. 9.4.2 take the new form

$$\theta(z) = \frac{DT_{sam}^2(z/2)(z+1)}{J(z-1)^3 + T_{sam}z(z-1)\left(K + K_d\frac{z-1}{z}\right)T_{sam}} \tag{9.4.7}$$

and

$$\lim_{n\to\infty} \theta(nT_{sam}) = \lim_{z\to 1} \frac{z-1}{z}\theta(z) = \frac{D}{K}. \tag{9.4.8}$$

Equation 9.4.8 shows that the steady-state angular error is no longer dependent on the sampling period T_{sam}.

Figure 9.4.5 presents a simulation of the control system with a PWM based on Eq. 9.4.5 (see Example 9.4.1). In this case $T_{sam} = 0.25$ sec, but the steady-state error is now equal to 0.456°, as predicted by Eq. 9.4.8.

Adding an Integrator to Nullify the Steady-State Error In orbit-maneuvering control tasks in which high thrust is activated for long periods (i.e., tens of minutes), it is of utmost importance to minimize the steady-state angular errors. This enables efficient orbit control with a minimal waste of fuel, as explained in Section 3.4.3.

The steady-state error due to the disturbance can be decreased to null by adding integration control error to the already existing position and derivative control errors. It is possible to add an integrator to the open-loop transfer function of the control loop without changing appreciably the high-range frequency characteristics.

The integrator is added with an appropriate low-frequency zero, as is usual with frequency design techniques.

EXAMPLE 9.4.1 *(Continued)* Since the crossover is $\omega_{co} = 0.75$ rad/sec (Figure 9.4.2), it is appropriate to add an integrator with a zero located at $\omega_z = 0.05$ rad/sec so that the higher-frequency range of the open-loop gain is not compromised. After the Tustin transformation, the revised discrete control network becomes

$$G_1 = \frac{z(1/\omega_z + T_{sam}) - 1/\omega_z + T_{sam}}{(z-1)/\omega_z} = \frac{z20.25 - 19.75}{20(z-1)}.$$

The results are given on the Nichols chart of Figure 9.4.6, where it can be clearly seen that the gain and phase margins have not deteriorated as a result of adding the integrator.

The time responses for the 1-N-m disturbance are shown in Figure 9.4.7 (overleaf). The time constant of the integrator control network is of the order of 20 sec, as expected ($\omega_z = 0.05$ rad/sec). The error is comparatively large only for the first 20 sec, which is a negligible time in view of the total duration of the ABM stage. For the rest of the time, the attitude error is null.

Sensor Noise Amplification One of the major problems in the design of feedback control systems is the amplification of sensor noise. This can result in saturation of torque controllers and thus prevent the feedback control system from operating satisfactorily. The effect is common to all controllers, but is seriously aggravated when the controller is based on liquid reaction thrusters. Unpredictable parasitic

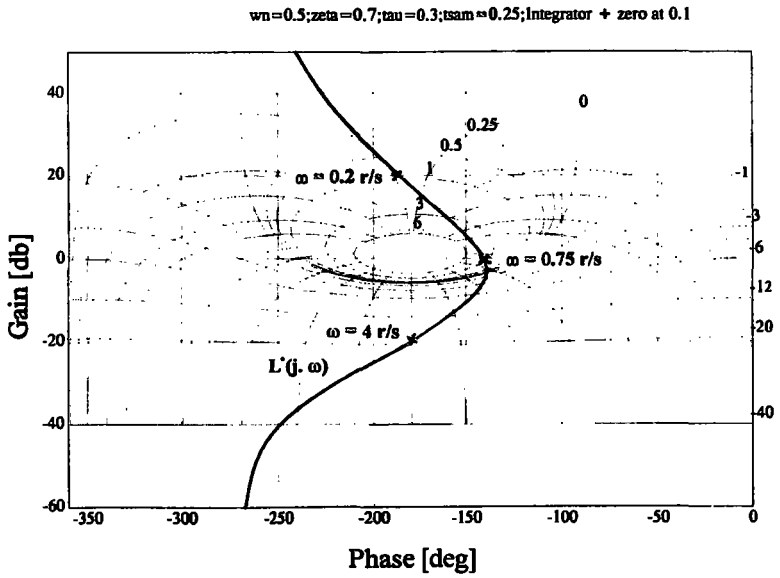

Figure 9.4.6 Adding an integrator as depicted on the frequency-domain chart.

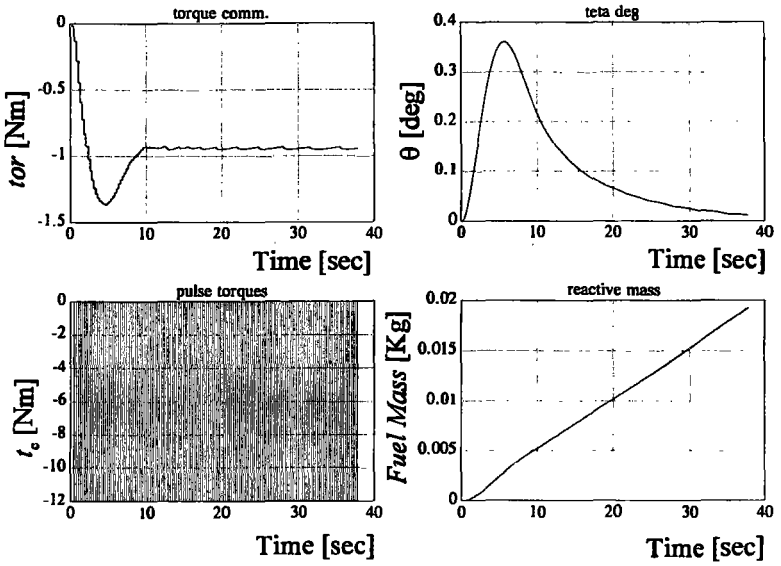

Figure 9.4.7 Time-domain results with the integrator added in order to nullify steady-state angular error.

waste of fuel shortens the mission lifetime of the satellite, which is intolerable from the system engineering point of view. Hence, even in the preliminary stages of designing a reaction attitude control loop, the amplification of sensor noise must be carefully considered and attenuated.

The first natural way to decrease noise amplification is to reduce the bandwidth of the feedback control system (at the expense of increasing the attitude errors due to external disturbances). This solution has the advantage of increasing the gain margins of the structural modes, a subject to be treated in Chapter 10. The second way to deal with the problem is to precede the PWM with an adequate dead zone, or to limit the minimum pulse width of the modulator output. There is also the possibility of using both techniques in conjunction. A compromise between attitude accuracy and fuel flow per unit time for a given level of sensor noise will help to fix the final bandwidth of the open-loop transfer function as well as the level of dead zone to be used (if any). These tradeoffs are clarified in the following example.

EXAMPLE 9.4.2 As in the previous example, $J = 500$ kg-m^2. We shall use a PW modulator to compute the on-time of the thrusters according to Eq. 9.4.6, so that T_{sam} has no influence on the steady-state angular error of the feedback control loop. No integrator is included in the control network. The sensor noise level of a good earth sensor (see Appendix B) - used to sense the attitude of the satellite in the orbit reference frame - ranges from 0.03° to 0.1° (RMS). In order to emphasize the effect of amplifying this noise, we will assume an exaggerated noise level of 0.3° (RMS). In the analysis to follow, $T_{sam} = 0.5$ sec and the disturbance level is $D = 1$ N-m.

In the first try, choose $\omega_n = 0.5$ rad/sec, $\xi = 0.7$, $\tau = 0.3$ sec, and $T_{sam} = 0.5$ sec. The open-loop gain of the solution is shown in Figure 9.4.8. With no sensor noise, the time history is shown in Figure 9.4.9. The steady-state error is 0.456°, as calcu-

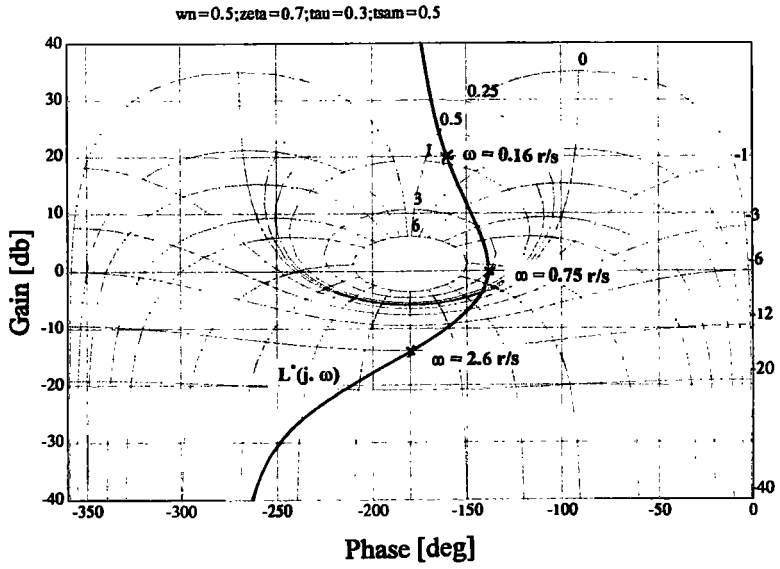

Figure 9.4.8 Open-loop transfer function for the feedback control with $\omega_n = 0.5$ rad/sec, $\xi = 0.7$, $\tau = 0.3$ sec, and $T_{sam} = 0.5$ sec.

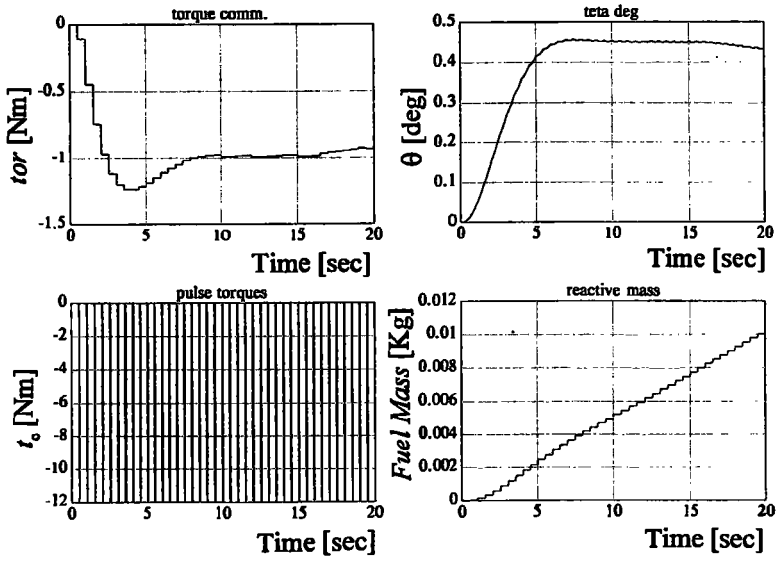

Figure 9.4.9 Time-domain results for a disturbance of 1 N-m without sensor noise; $\omega_n = 0.5$ rad/sec, $\xi = 0.7$, $\tau = 0.3$ sec, and $T_{sam} = 0.5$ sec.

lated from Eq. 9.4.8. The theoretical noise amplification was calculated to be *tor/* noise = 11.848 (RMS). The fuel consumption rate is 0.5 g/sec. Amplification of sensor noise augments the attitude error as shown in Figure 9.4.10 (overleaf), where peak errors as high as 0.9° may be perceived. Even if so much angular error is acceptable, quadrupling the rate of fuel mass consumption (to 2 g/sec) is not.

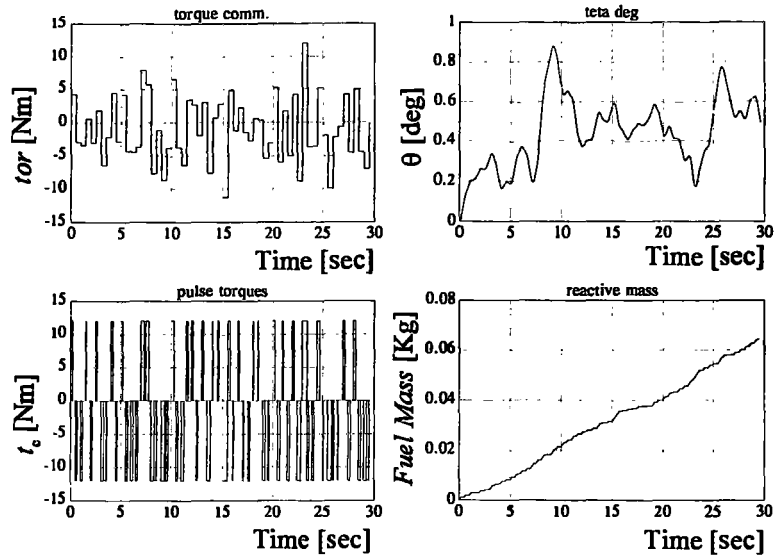

Figure 9.4.10 Time-domain results for a disturbance of 1 N-m with sensor noise of 0.3° (RMS); $\omega_n = 0.5$ rad/sec, $\xi = 0.7$, $\tau = 0.3$ sec, and $T_{sam} = 0.5$ sec.

Let us diminish the sensor noise amplification, and also the fuel consumption, by reducing the bandwidth of the attitude control loop to $\omega_n = 0.3$ rad/sec. Of course, we can increase the time constant of the noise filter to $\tau = 0.7$ sec. The theoretical noise amplification is now only *tor*/noise = 2.6 (RMS), a reduction by a factor of 4.5. With no noise, the consumption of fuel remains exactly as for the case with $\omega_n = 0.5$ rad/sec, since the fuel consumption rate depends only on the level of disturbance and not on the bandwidth of the control loop. The steady-state error due to the disturbance of 1 N-m is now higher: 1.21°, as predicted by Eq. 9.4.8 (see also Figure 9.4.11). With application of the same sensor noise, the attitude error now increases to about 1.7° with fuel consumption of 0.75 g/sec, which is higher by only 50% than the fuel consumption without sensor noise (see Figure 9.4.12).

The second proposal for decreasing fuel consumption was to insert a dead zone before the PWM. Suppose we use a dead zone of 3 N-m. The results in the time domain with $\omega_n = 0.5$ rad/sec show that the fuel consumption rate is now only 1.1 g/sec, compared to 2 g/sec without the dead zone, and with no significant increase in peak attitude errors.

We conclude that tradeoffs similar to those described here are necessary to achieve the best possible design results for the attitude control problems given under various mission constraints. The results of our analysis are summarized in Table 9.4.2.

Input-Output Behavior of a Reaction ACS

In classical continuous feedback theory, there is a high correlation between (a) the time response $\theta(t)$ of the output to a step input and (b) the closed-loop frequency response $T(s) = \theta(s)/\theta_{com}(s)$, where $\theta_{com}(s)$ is a step command input (see Horowitz 1963, Sidi 1973). This relationship is seriously distorted for sampled systems

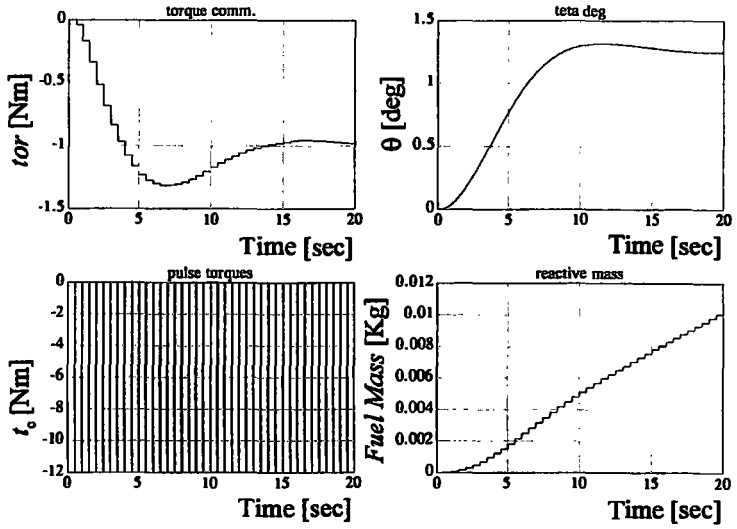

Figure 9.4.11 Time-domain results for a disturbance of 1 N-m without sensor noise; $\omega_n = 0.3$ rad/sec, $\xi = 0.7$, $\tau = 0.7$ sec, and $T_{sam} = 0.5$ sec.

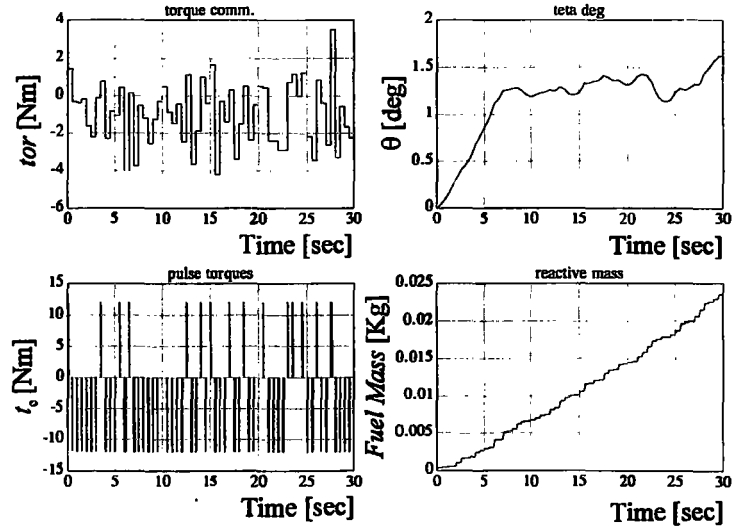

Figure 9.4.12 Time-domain results for a disturbance of 1 N-m with sensor noise of 0.3° (RMS); $\omega_n = 0.3$ rad/sec, $\xi = 0.7$, $\tau = 0.7$ sec, and $T_{sam} = 0.5$ sec.

Table 9.4.2 *Results of tradeoff to reduce sensor noise amplification* ($\xi = 0.7$, disturbance $= D = 1$ N-m)

Figure	ω_n [r/sec]	τ [sec]	K	K_d	Dead Zone [Nm]	Sensor Noise RMS [deg]	Noise Amplific.	Peak Error [deg]	Fuel Rate Consumption [gr/sec]
9.4.9	0.5	0.3	125	350	0	0	—	0.46	0.5
9.4.10	0.5	0.3	125	350	0	0.3	11.85	0.9	2.18
9.4.11	0.3	0.7	45	210	0	0	—	1.3	0.5
9.4.12	0.3	0.7	45	210	0	0.3	2.6	1.7	0.7
	0.5	0.3	125	350	3	0.3	—	1.05	1.17

if no special care is taken when defining the input-output transfer function. The transfer function for a digital, sampled feedback control loop can be designed in various equivalent ways (see Saucedo and Schiring 1968, Sidi 1977). We can put:

$$T(z)_{z=e^{sT_{sam}}} \equiv T^*(s)_{s=j\omega} \equiv T(w)_{w=(z-1)/(z+1)}, \tag{9.4.9}$$

where * denotes "sampling process" in the continuous frequency domain, "s" is the Laplace transform variable, z is the Z transform variable, and w is the W (bilinear transformation) variable. We also have

$$\frac{\theta(z)}{\theta_{com}(z)} \equiv \frac{\theta^*(s)}{\theta^*_{com}(s)} \equiv \frac{\theta(w)}{\theta_{com}(w)}. \tag{9.4.10}$$

The frequency response of the sampled transfer function in Eq. 9.4.10 does not correlate well with the step time response, as in continuous systems (see Horowitz 1963). We can alleviate this difficulty by defining a mixed transfer function:

$$T = \frac{\theta(s)}{\theta^*_{com}(s)}. \tag{9.4.11}$$

The output of interest in Figure 9.4.1 is the continuous output $\theta(t)$, not $\theta^*(t)$. With this practical definition, it has been shown (Sidi 1977) that the approximate relationship between the time response of the output and the frequency response of the transfer function remains as good as for continuous feedback systems. With this assumption, it is much easier to define the desired input-output transfer function in the w frequency domain for a desired time response of a sampled feedback control loop (see Saucedo and Schiring 1968). This approach will be followed here.

Dead Zone and Minimum Impulse Bit of the Reaction Pulses Because of engineering constraints, there is a minimum pulse duration Δt_{min} that reaction thrusters can deliver. The minimum impulse bit $F(\Delta t_{min})$, multiplied by the torque arm Δ of the thrusters, is the minimum torque impulse bit (MTIB) delivered to the satellite at the sampling instance: $\Delta F(\Delta t_{min})$. Between two sampling events, the attitude control system is in open loop. During the period that the torque exists (designated by tp), angular velocity will increase by

$$\Delta\dot{\theta} = \frac{F\Delta tp}{J}, \tag{9.4.12}$$

where F is the thrust of the reaction thruster, Δ the torque arm, and J the moment of inertia about the axis of rotation. Until the next sampling (in T_{sam} sec), the attitude will increase by

$$\Delta\theta = \frac{F\Delta tp}{J}(T_{sam} - tp). \tag{9.4.13}$$

This equation is self-explanatory: $\Delta\theta$ is the minimum possible magnitude change of θ. However, it is important to emphasize that precise attitude control will demand very low impulse bits.

Unfortunately, things are not quite so simple. The basic relationship for attainable accuracy stems from Eq. 9.4.4 or Eq. 9.4.6. We shall concentrate on Eq. 9.4.6, the equation of the PW modulator. This modulator will deliver a pulse torque proportional to the torque command calculated in $G(z)$ of Figure 9.4.1. After the transient

period in response to the step command (or whatever command it may be), the steady-state error is $e_{ss} = \theta_{com} - \theta_{ss}$. This error will be translated by $G(z)$ to a steady-state torque command, tor_{ss}. In these special circumstances - when the error is not continuous because of the sampling process - we shall rather speak of a minimum error e_{min} and a minimum torque tor_{min}. For a minimum pulse width tp_{min}, the minimum torque that will activate the PW modulator is

$$tor_{min} = \frac{tp_{min} F \Delta}{T_{sam}} = e_{min} K. \tag{9.4.14}$$

From this equation it readily follows that

$$e_{min} = \frac{tp_{min} F \Delta}{T_{sam} K} = \frac{\text{MTIB}}{T_{sam} K}. \tag{9.4.15}$$

In Eq. 9.4.15, MTIB is the *minimum torque impulse bit* that the reaction thruster can deliver to the satellite about the controlled axis. This term deserves some special attention: $\text{MIB} = tp_{min} F$ is a technical characteristic of the thruster - namely, its minimum impulse bit. The torque period tp is highly dependent on the chemical composition of the propellant (see Appendix C). The thrust level F also cannot be chosen at will; for instance, F is of the order of 10 N for bipropellant propulsion systems. For monopropellant propulsion systems such as hydrazine thrusters, much lower thrusts are common. Still, the term $tp_{min} F$ is of utmost importance, as can be seen in Eq. 9.4.15. The minimum tp_{min} is equivalent to a torque dead zone, with all the relevant implications such as limit cycling.

The torque impulse bit is related to the torque arm Δ. Practically, this term can be adapted as desired by correctly locating the thruster on the satellite, as explained in Section 9.2.1. The error term e_{mln} of Eq. 9.4.15 can also be expressed in terms of ω_n, the natural frequency of the second-order model feedback control system of Figure 9.4.1, in which $K = \omega_n^2 J$.

EXAMPLE 9.4.3 In this example, $J = 500$ k-m^2. We will show the relationship between the steady-state attitude error and the MTIB factor. In order to perceive clearly this error, the closed-loop control system will be subjected to a small attitude command, let us say $\theta_{com} = 0.1°$. We choose $\omega_n = 1$ rad/sec, $\xi = 0.7$, and $\tau = 0.3$ sec, so that $K = 500$, $K_d = 700$, and $T_{sam} = 0.25$ sec.

Figure 9.4.13 (overleaf) shows the time response results for $F = 6$ N, $\Delta = 1$ m, and $tp_{min} = 0.01$ sec: $\text{MTIB} = 6 \times 0.01 = 0.06$ N-m-sec. With this data, according to Eq. 9.4.15, $e_{min} = 0.06/(0.25 \times 500) = 4.8 \times 10^{-4}$ rad $= 0.0275°$. This analytical result is clearly confirmed by the time-domain simulation, the results of which are shown in the figure.

To increase the accuracy, we could decrease F or Δ or both. Suppose that $F = 2$ N. Hence MTIB = 0.02 N-m-sec and, by Eq. 9.4.15, e_{min} is reduced to $e_{min} = 0.0092°$. The time-response results agree with Eq. 9.4.15 (see Figure 9.4.14, overleaf). Suppose once again that $F = 2$ N but that now $\theta_{com} = 1°$. This makes the transient in the error torque command relatively large (as compared to the maximum torque that the reaction thruster can provide), so the torque controller is saturated and hence the time response is more sluggish; see Figure 9.4.15 (page 287). (Of course, the situation could be partially improved by increasing Δ and hence also the torque reaction level

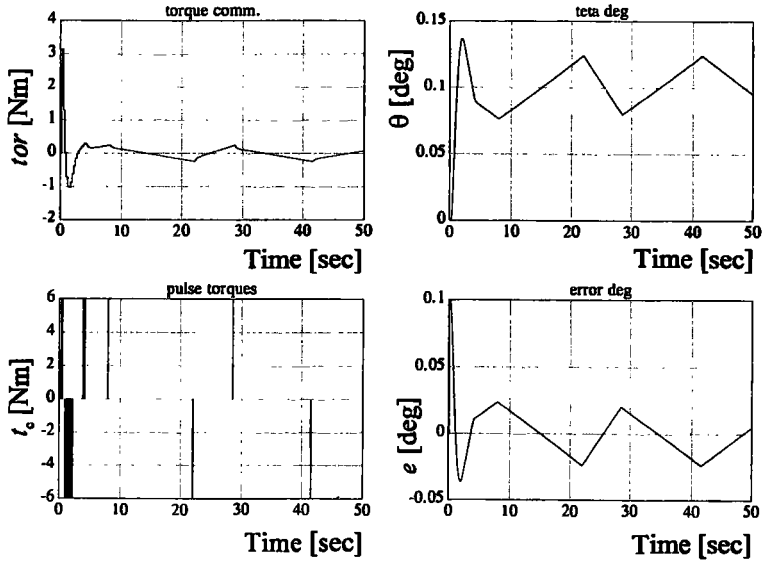

Figure 9.4.13 Time-domain results for the case in which $F\Delta = 6$ N-m, $tp_{min} = 0.01$ sec, $\omega_n = 1$ rad/sec, $K = 500$, $T_{sam} = 0.25$ sec, and $\theta_{com} = 0.1°$.

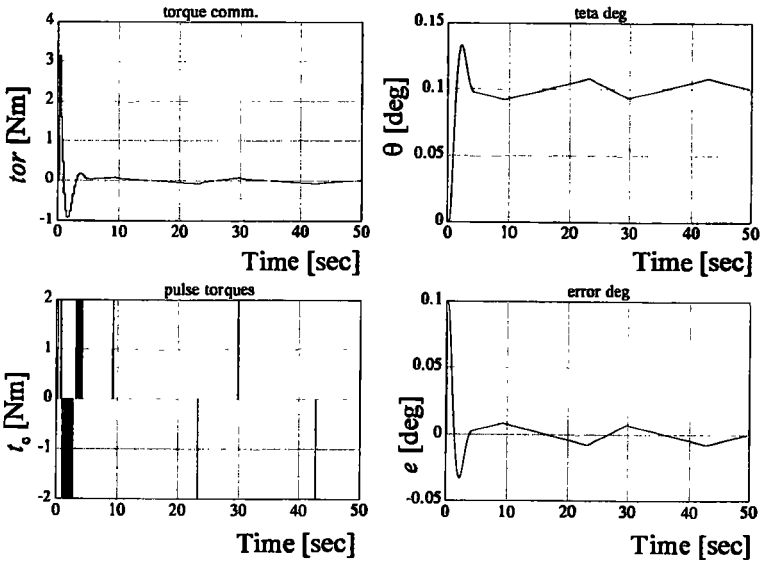

Figure 9.4.14 Time-domain results for the case in which $F\Delta = 2$ N-m, $tp_{min} = 0.01$ sec, $\omega_n = 1$ rad/sec, $K = 500$, $T_{sam} = 0.25$ sec, and $\theta_{com} = 0.1°$.

$F\Delta$. But doing so would increase the steady-state error, which is contrary to our primary desire for attitude accuracy.) To overcome this phenomenon and improve the time response, we must use nonlinear design techniques such as those presented in Section 7.6.

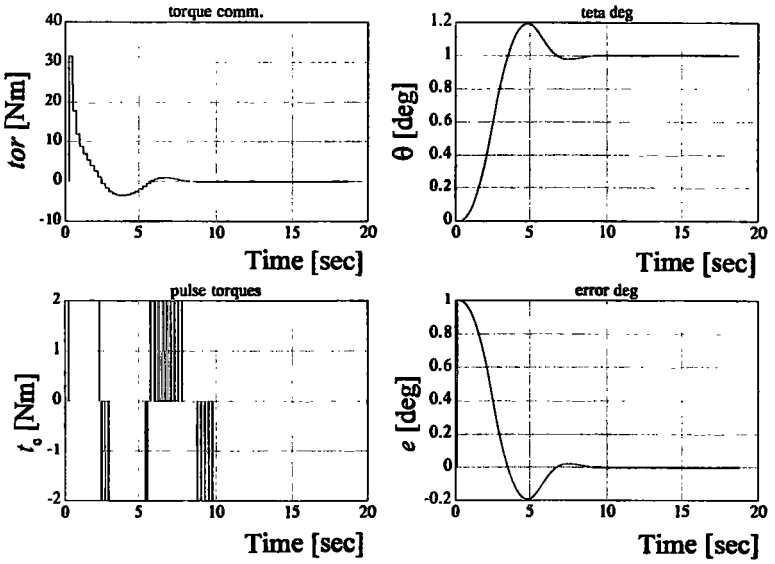

Figure 9.4.15 Time-domain results for the case in which $F\Delta = 2$ N-m, $tp_{min} = 0.01$ sec, $\omega_n = 1$ rad/sec, $K = 500$, $T_{sam} = 0.25$ sec, and $\theta_{com} = 1°$.

It is important to notice that the attitude error and output responses need not follow exactly the time histories shown in Figures 9.4.13, 9.4.14, and 9.4.15. The minimum values of the errors are guaranteed (as per Eq. 9.4.15), but these errors can reach their limiting values at different times according to the initial values $\theta(0)$ and $\dot{\theta}(0)$ of the system and according also to the level of the attitude input command.

9.5 Reaction Control System Using Only Four Thrusters

In Section 9.2 (see esp. Figure 9.2.3), six thrusters were used to implement a reaction control system for attitude and orbit control. For these two purposes, the six thruster jets provided the necessary positive and negative torques about the three body axes (for attitude control) as well as linear velocity changes along the $\mathbf{X}_B$ and the $-\mathbf{Y}_B$ axes (for orbit control). It is possible to achieve three-axis attitude control by using only four thrusters. However, with such a reaction control system, the possibility of achieving linear velocity augmentation in desired body directions is no longer available. This is the principal drawback in using a limited number of thrusters (fewer than six).

Figure 9.5.1 (overleaf) shows the torque vector arrangement obtained by using four thrusters. As shown in the figure, each thruster provides a positive torque in a given direction with respect to the satellite body; these torques are denoted T_1, T_2, T_3, and T_4. In Figure 9.5.1, with directions of the torques produced by each one of the thrusters defined in the body frame, every vector control command torque $\mathbf{T}_c$ can be achieved with three of the four available torques. Since the torques produced by each thruster have constant torque levels, the on-time must be computed for each of the thrusters Ti_i, $i = 1, \ldots, 4$ (cf. Section 9.2). The transformation between the control torque components in the body axis frame and the on-time of each thruster can be written in the following matrix form: